Comparative Performance of Philic and Phobic Oil-Mist Filters

Benjamin J. Mullins and Ryan Mead-Hunter
School of Public Health, Faculty of Health Sciences, Curtin University, GPO Box U1987, Perth WA 6845, Australia

Fluid Dynamics Research Group, Curtin University, GPO Box U1987, Perth WA 6845, Australia

Renato N. Pitta and Gerhard Kasper
Institute for Mechanical Process Engineering and Mechanics (MVM), Karlsruhe Institute of Technology, D-76131 Karlsruhe, Germany

Wolfgang Heikamp
Rhodius GmbH, D-91781, Weißenburg, Germany

DOI 10.1002/aic.14479
Published online May 6, 2014 in Wiley Online Library (wileyonlinelibrary.com)

The evolution of pressure drop, drainage rate, saturation, and efficiency of combined philic, and phobic oil mist filters in real-time are examined. The experiments used four different filter configurations, with a combination of oleophobic and oleophilic fibrous filter media, and one oleophilic only reference. The effect of separating filter materials of differing wettability, with a mesh, was also explored. It was found that inclusion of a mesh between layers promoted increased drainage rates and resulted in a significantly lower pressure drop across the filter. The overall mass-based filtration efficiency was also slightly higher for the configurations containing the mesh. Conversely, re-entrainment of droplets from the rear face of the filter was only observed in filter configurations without the central mesh. Filters with oleophobic initial layers did not display a classical "depth filtration" pressure drop curve. The oleophobic media was found to possess lower steady-state saturation than oleophilic media. Additionally, the steady-state saturation of the oleophilic filter media, when placed at the rear of the filter, was lower when the central mesh was present. The saturation values were compared with recently published theory. © 2014 American Institute of Chemical Engineers *AIChE J*, 60: 2976–2984, 2014
Keywords: oil-mist, filter, saturation, equilibrium, efficiency

Introduction

The effective and efficient separation of liquid aerosols or mists is of significant importance to many process and automotive applications and also relevant to many other technologies such as mist eliminators and fuel cell dewatering, for example. Liquid aerosols are typically generated by industrial compressors, lubricated machining and cutting processes, and in engine crankcases. One of the most effective and commonly used methods to treat oil-mist is through the use of fibrous filters.

Most industrial oil-mist filters are oleophilic, with relatively well described, though difficult to accurately model, behavior.[1–4] Such filters will rapidly become clogged with oil, causing an increase in pressure drop and (usually) a decrease in efficiency, until they attain a state of equilibrium. This process has been described in the literature,[1–3,5–9] with several authors describing the process by which a clean filter reaches the equilibrium state, in terms of a number of stages. Although some of the mist filters used in industry have been constructed of oleophobic fibers, or a combination of philic and phobic media, phobic filters have not yet received significant attention in the literature.

The use of oleophobic filters may, in theory, act to reduce saturation as, due to lower surface energy, the coalesced oil will not fully wet the media. Given the lower surface energy, however, such media may also be more likely to allow collected oil to be "blown off" or re-entrained into the gas stream from the rear of the filter.

The state of being (oleo)phobic or (hydro)phobic, with respect to fibers, is generally defined by the presence of clamshell droplets, with a contact angle between $\sim 60^{\circ}$ and 180°, the latter generally being regarded as "super"-()phobic.

Thus far, there have been relatively few works that have examined oleophobic fibers and/or filter media.[10–14] Most of these works have only considered aerosol/droplets on single phobic fibers,[10,13] the capillarity of phobic media,[11] or filter surface energy measurements.[12] However, the performance of phobic media as used in mist filters, has received little attention.

While there have been some studies that have considered the use of combined philic–phobic media for liquid–liquid

Correspondence concerning this article should be addressed to R. Mead-Hunter at r.mead-hunter@curtin.edu.au.

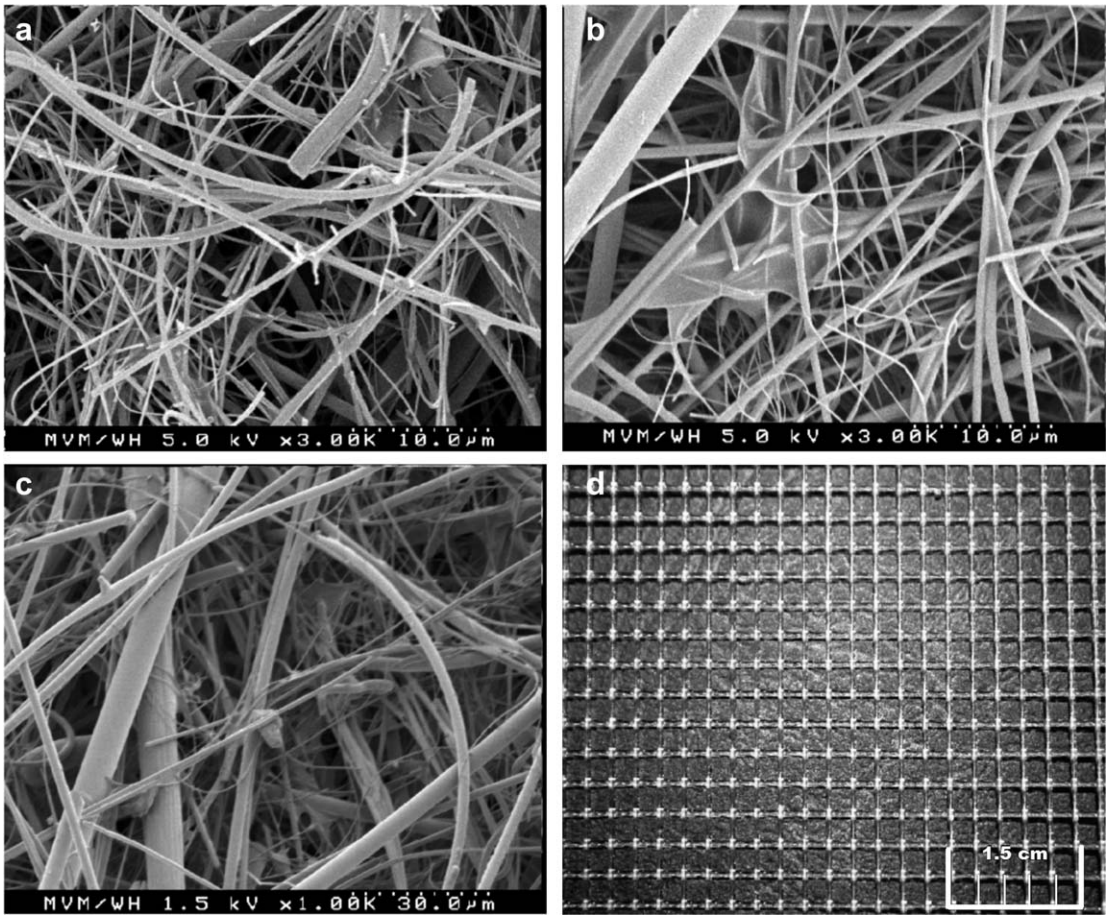

Figure 1. SEM images of the filters used and the supporting mesh, (a) Phil01, (b) Phil02, (c) Phob01, and (d) the mesh support.

separation,[15] there has been little work done in regard to the application of such combined media to the treatment of liquid aerosols.

To the best of our knowledge, only one other work[16] has considered filters composed of both philic and phobic media for the treatment of aerosols. In their work, however, Agranovski et al.[16] used a "nonwettable" media with fiber diameters nearly four times larger than the fibers in the "wettable" media, producing substantially different collection efficiencies, which may indicate why no improvement was found when using a nonwettable layer followed by a wettable layer. More importantly, the definition of "nonwettable" used by Agranovski et al.,[16] Agranovski and Shapiro,[17] Agranovski and Braddock,[18] Agranovski and Shapiro[19] was the formation of barrel-shaped droplets (and "wettable" defined as forming a film), which does not agree with the definition used by other authors.[10,13,20,21] Therefore, these works can be considered to have used "super"-philic and philic media, not phobic. Additionally, oils wet a surface more readily than water, so a "nonwettable" filter for aqueous aerosols may still be wetted by an oil aerosol.

This work will, therefore, provide a more comprehensive study of true philic and phobic media. Such work will be of potential benefit to industry, where filters composed of philic, phobic, or combinations of both media types are used, often with little supporting evidence, as well as advancing our fundamental knowledge of the physics of philic/phobic mist filter systems.

The use of layers of both philic and phobic media together may act to improve filter performance using the advantages offered by each respective media type (or the opposite). This work will, therefore, attempt to find if such a combination of layers is beneficial—and if so, what the preferential configuration is. Factors to consider are the ordering of media wettability and the location of (any) supporting or space structures (mesh in our case); which when situated between filter layers may act to promote internal drainage, thereby reducing transport of coalesced fluid to the rear of the filter.

In summary, it is hypothesized that the inclusion of mesh between layers in a combined philic–phobic mist filter will reduce pressure drop, increase efficiency and reduce re-entrainment (if it can be detected).

Experimental

Filters

The filters used in this work were all constructed from layers of commercially available glass filter media (Hollingsworth and Vose, East Walpole). Scanning electron microscope (SEM) images of the filters used are shown in Figures 1a–c. The filters in Figures 1a,b are both oleophilic, whereas the filter shown in 1c was coated with a fluorinated polymer during the manufacturing process, to render it oleophobic. As the filters are thin, and composed of very fine fibers, they have relatively low structural integrity and need to be supported by a mesh (or perforated plate) backing. The mesh

Table 1. Filter Properties, with ± Indicating Standard Deviation

Filter	Z (mm)	α (−)	d_{fav} (μm)	θ (°)	d_{fmin}	d_{fmax}
Phob01	0.46 ± 0.05	0.073 ± 0.001	3.4 ± 2.2	≥ 86	0.2	3.79
Phil01	0.60 ± 0.05	0.05 ± 0.02	0.67 ± 0.62	≤ 15	0.11	1.37
Phil02	0.60 ± 0.05	0.06 ± 0.02	0.66 ± 0.76	≤ 15	0.1	1.44

used in these experiments is shown in Figure 1d. The mesh used was polyester and had an approximate contact angle (θ) of 30° with the oil used.

All filters used possess a bimodal fiber diameter distribution. Table 1 shows the filter properties, with Z the filter thickness, α the packing density, d_{fav} the average fiber diameter, d_{fmin} the mode of the smaller fiber diameter group, d_{fmax} the mode of the larger fiber diameter group, and θ the contact angle between the fiber and the oil used.

Fiber diameters were measured from the SEM images of a random sample of 100 fibers for each filter. The filter face area of each filter was of 72 cm^2. The packing density of each filter was calculated using the formula

$$\alpha = \frac{m_f}{V\rho_f} \quad (1)$$

where m_f is the mass of the fibers in the filter, V is the volume of the filter, and ρ_f is the density of the fibers. A small amount of error in this measurement would exist due to the polymer binder and/or copolymer coating. However, this would be small as the polymer density is much lower than that of glass. The standard deviations given in Table 1 for d_f are large due to the broad fiber diameter distribution, dominated by finer fibers.

Contact angle measurements for the philic media and the mesh are reported from measurements on individual fibers, as per previous work.[22] For the phobic media, contact angles were determined using the same method and also using sessile drops on the surface of the media, as per the method in Ref. [10].

Filter configurations

The experiments were conducted using four layers of filter media (except in the philic only case, where five layers were used) and one or two supporting meshes. The combinations used are shown in Table 2. With the exception of Configurations 1B and 2B, all configurations had a layer of supporting mesh located after the final media layer.

Apparatus

The experimental apparatus is shown in Figure 2. All experiments were conducted using Sigma Light Mineral Oil (M3516, Sigma-Aldrich, Germany), with aerosol generated using a Collison nebulizer. Make-up compressed air was presaturated using the same oil, to ensure no evaporation of the aerosol during the experiments.

Two load cells (Transducer Techniques, CA) were used to record the mass of the test filter chamber and the high efficiency particulate air (HEPA) filter located after the test filter. To permit real time gravimetric measurements, the filter chambers were connected to the ducting by flexible joints which allow the filter to exert a force on the load cell as it captured oil droplets. The changes in the mass of the filters as they are loaded with particles permitted filter saturation and filter collection efficiency (provided the influent mass loading is known) to be measured over time.

Two balances (AnD, Japan) were used to continuously measure the amount of oil drained from the bottom of the test filters into two closed receptacles, one immediately before and one immediately after the filter, to measure the drainage rate during the experiments. The balances allow the drainage rate from the filter to be quantified in real time. The connections between the filter chamber and the drainage vessels were kept as short as possible to minimize the time delay between the liquid leaving the filter and being measured by the balance.

A differential pressure piezoelectric transducer (RS Components, Germany) was used in the filter chamber to continuously measure filter pressure drop.

Optical particle counters (OPCs, University of Karlsruhe) were used to measure the larger diameter aerosols before and after the filter. These instruments are described in Sachweh et al.,[23] Heim et al.,[24] and Mullins et al.[25] The instruments were calibrated for the oil aerosol used as per the method of Heim et al.[24]

A scanning mobility particle sizer (SMPS) consisting of a TSI 3010 Condensation particle counter (CPC, TSI, MN) and Hauke long differential mobility analyzer (Hauke, Austria) was used to measure aerosols between 10 nm and 1 μm before and after the test filters. The OPCs and SMPS both measure in 0.3–1.0 μm size range and the OPC measures up to at least 10 μm in the configuration used. As the oil aerosol is spherical and of known density and refractive index, the two instrument types showed excellent agreement, once the OPC count efficiency was corrected as per Heim et al.[24] A process aerosol monitor (PAM 510, Topas, Dresden) was also used after the nebulizer to ensure the particle generation rate remained constant.

Procedure

All experiments were conducted with a constant flow rate of 10.7 L/min (with a filter face velocity of 0.248 m/s), regulated using a critical orifice upstream of the pump. SMPS/OPC measurements were started immediately after aerosol generation was commenced. It was found that particle concentrations before the filter were constant, so SMPS measurements before the filter were only taken every 4 h, while measurements after the filter were taken at 30 min intervals (averaging four SMPS scans per measurement). The OPCs

Table 2. Filter Configurations

Layer	1A	1B	2A	2B	3
First (Front)	Phob01	Phob01	Phil02	Phil01	Phil01
Second	Phob01	Phob01	Phil02	Phil01	Phil01
Third	Mesh	Phil02	Mesh	Phob01	Phil01
Fourth	Phil02	Phil02	Phob01	Phob01	Phil01
Fifth	Phil02	Mesh	Phob01	Mesh	Phil01

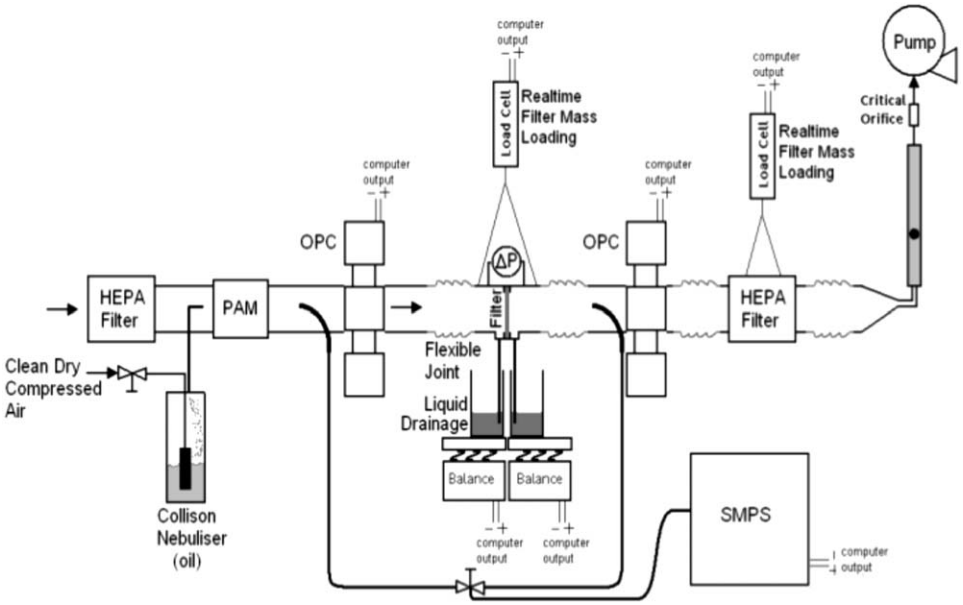

Figure 2. Schematic of the experimental setup.

were set to perform measurements for 5 min every 30 min for the duration of the experiment. Each of the filter configurations (as listed in Table 2) were tested twice.

During the experiment, the filter mass, pressure drop, and drainage oil mass were monitored to determine when filter reached equilibrium saturation (denoted by constant pressure drop and filter mass and also constant drainage rate). The filters reached equilibrium saturation between 8 and 10 h for all four experiments. The experiments were then continued for at least 24 h to confirm that an equilibrium had been reached and to allow observation of re-entrainment, if it occurred.

At the end of each experiment, the aerosol flow was stopped and the individual filter layers were carefully taken apart and weighed to allow determination of equilibrium saturation (S), of each individual layer.

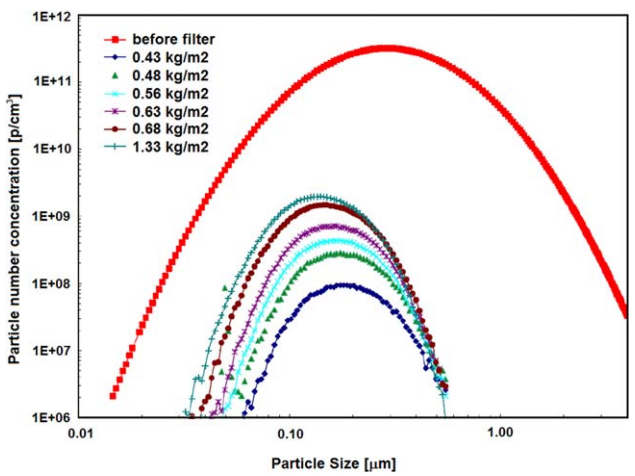

Figure 3. Particle size distributions before (as generated by the nebulizer) and after the filter during loading, (data shown is for Configuration 2A).

[Color figure can be viewed in the online issue, which is available at wileyonlinelibrary.com.]

Results

Figure 3 shows a typical particle distribution before and after the filter during loading.

Figure 4 shows the change in filtration efficiency over time for experiments using Configuration A. All five filter configurations were effectively 99.9999% efficient when new/clean.

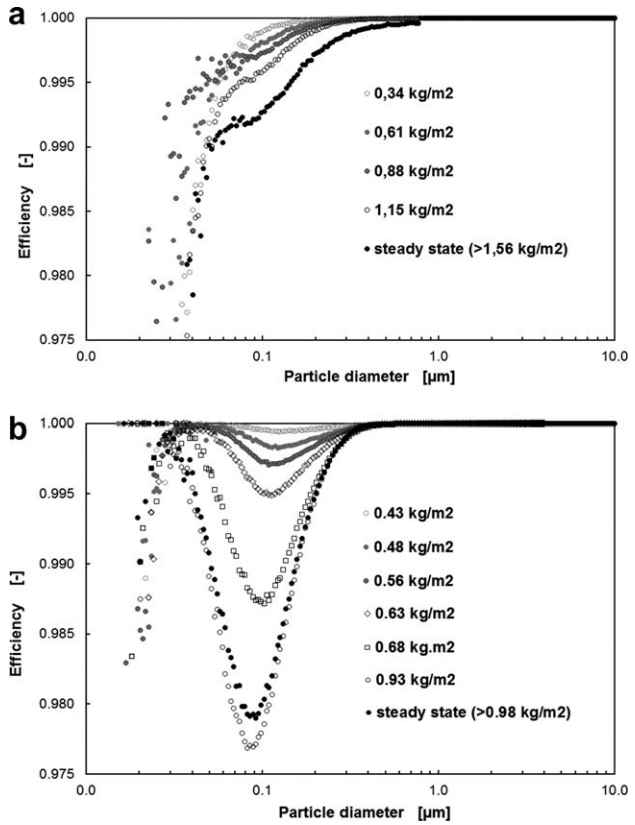

Figure 4. Particle capture efficiency with loading for Configurations 1A (a) and 2A (b).

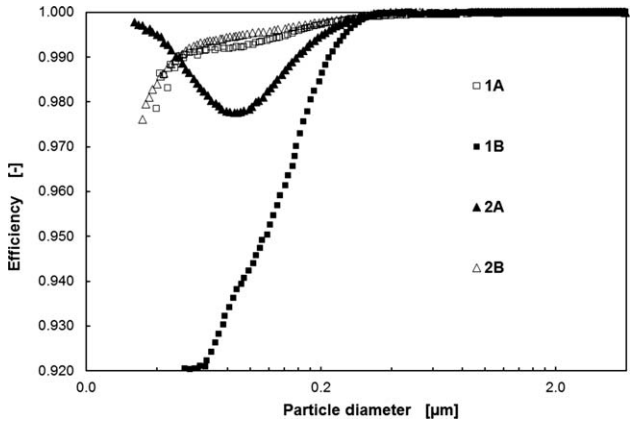

Figure 5. Total efficiency of each filter configuration, measured by SMPS/OPC system, at steady state.

The particle capture efficiencies for Configurations 1A and 2A are shown in Figure 4. Capture efficiencies for Configurations 1B and 2B have not been included, due to insufficient scanning during the loading phase of the tests on these configurations.

The total efficiency for each droplet size is shown in Figure 5. Given the re-entrainment observed for 2B, the efficiencies calculated from SMPS and OPC data are only accurate for the size ranges measured by the devices. For this reason, filter efficiencies were also determined gravimetrically, by considering the mass of oil collected in the HEPA filter downstream from the test filter chamber. Thereby accounting for any oil mass in droplets above the detection limit of the SMPS or OPC, but which did not settle out in the chamber.

Both gravimetric and OPC/SMPS datasets are included, as both measurement methods (White light OPC and Gravimetric) are included in relevant standards for mist filter testing (e.g., ISO 8573). This, therefore, highlights the limitations with both methods. Gravimetric measurement of liquid mists can also suffer from entrainment, or liquid transport to the filter holder.

Figure 6 shows the average pressure drop, drainage, and saturation results for each of the four mixed media experimental configurations. S_F is filter saturation, given as a fraction of the void space filled, D is filter drained oil mass, expressed as a percentage of the mass of oil in the filter at 100% of S_F and ΔP is pressure drop across the filter. These are plotted in terms of the cumulative mass loading per unit filter face area. This method is believed to be first used by Ref. [3] and is useful as it allows experiments conducted at different loading rates to be compared. If the loading rate is known then the x axis can be readily converted back to time. The experiments using the B configuration were run for longer total times, to allow any re-entrainment of particles to be observed, and so show data for higher cumulative mass loading than the experiment using Configuration A. Different experiment durations do not influence the results though, as the filters reach a steady state, and the mass loading rate was constant for all experiments.

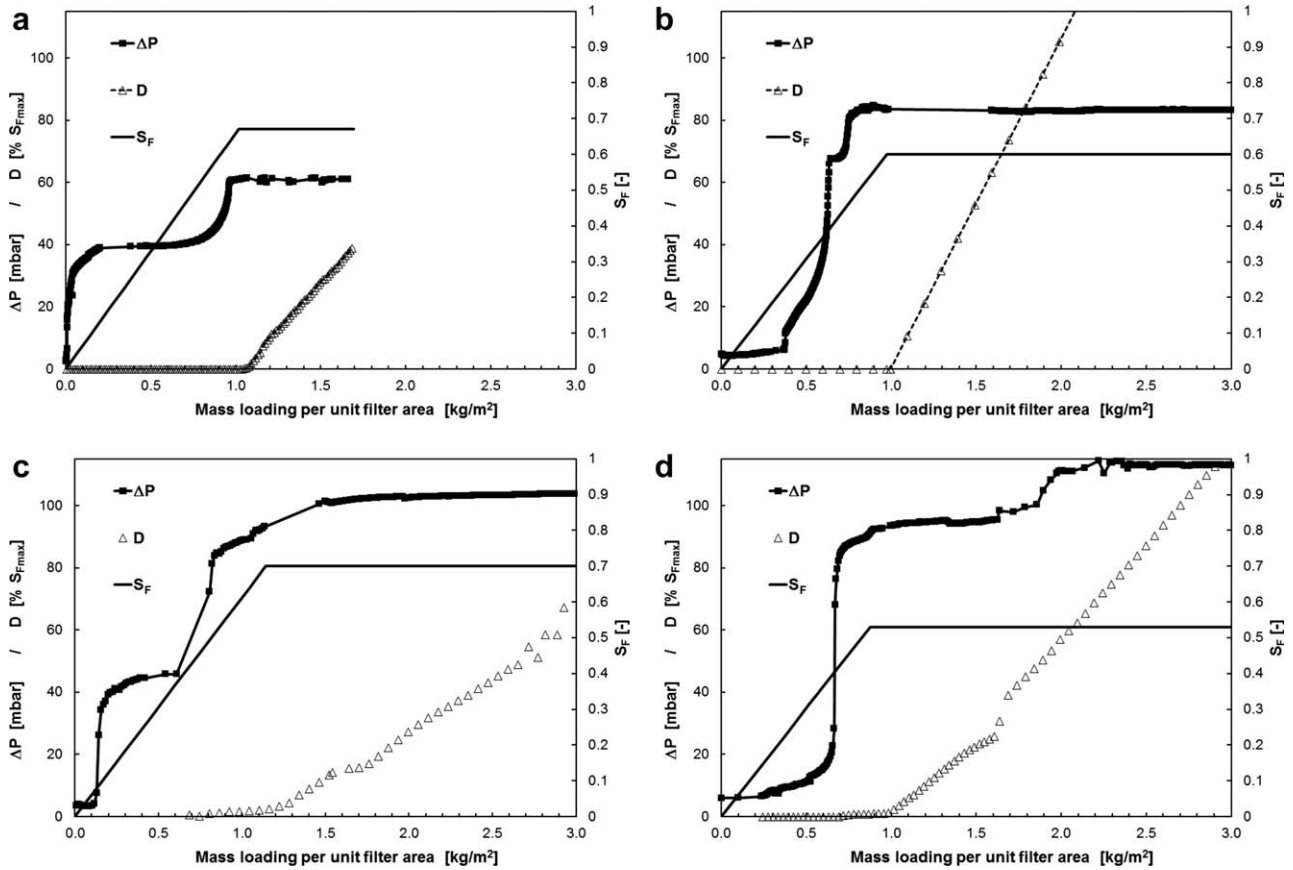

Figure 6. Pressure drop, drainage, and saturation curves for the different filter configurations, (a) 1A, (b) 1B, (c) 2A, and (d) 2B.

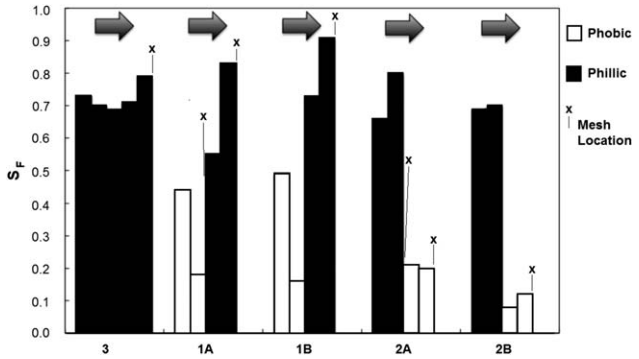

Figure 7. Equilibrium saturation of each layer in each filter configuration.

Arrows indicate airflow direction through each filter. A small amount of oil remained on the mesh layers, so the values are slightly lower than those in Figure 6.

For all experiments, there was no significant drainage from the front of the filter, with >99% of drainage by mass, collected after the filter.

Equilibrium saturation values were measured after the experiments for each layer in each experimental configuration. As expected, each layer reached a different level of saturation, depending on the material type and its location within the test filter. These data are shown in Figure 7.

Discussion

It can be seen from data presented in Figure 3 that the particle concentration after the filter increases during loading, and the mode of the distribution becomes smaller. The filtration efficiency decreases with time due to the coalesced liquid increasing the effective local or global fiber diameter and decreasing the residence time for particles within the filter.

As expected, the filtration efficiency decreases as the filter is loaded with oil and reaches a constant value after the system has reached equilibrium (this is shown in Figure 4). This corresponds with most mist filter efficiency results reported previously (when measured accurately at small particle sizes).

Figure 4b demonstrates the effect of diffusional capture of small particles, where the capture efficiency is high for particles smaller than the most penetrating particle size (MPSS). The change in efficiency with loading is largely as expected for a typical mist filter.

Figure 4a, however, shows an MPPS that corresponds to the smallest particle size, suggesting poor diffusional capture of droplets. This is most likely due to re-entrainment of small particles—possibly caused by bubbles bursting on the rear face of the filter. A less likely possibility is recondensation of fine aerosol particles, however, the oil used has a low vapor pressure, which should result in very low evaporation rates. Re-entrainment will be discussed in more detail later.

The total mass based efficiencies at steady state (measured gravimetrically) are shown in Table 3, both Configurations 1A and 2A reach comparable efficiencies at equilibrium. The efficiency drop for 2A occurs at a lower mass loading than that of 1A, this can be explained by comparison of Figures 4a,b. While Figure 4b shows a consistently larger MPSS, than that in Figure 4a, it is difficult to discern what the MPSS for Configuration 1A (Figure 4a) is. Overall, there appears to be an efficiency reduction over the majority of particle sizes in Configuration 1A when compared to Configuration 2A.

Figure 4 also indicates that in Configuration 2A, the minimum total efficiency occurs before equilibrium is reached, with a slightly higher efficiency, this agrees with the observations of Ref. [3] on oleophilic media.

The most significant difference between the experimental configurations is the evolution of the pressure drop curve. Figures 6a,c show significantly lower equilibrium pressure drop values than Figures 6b,d due to the location of the supporting mesh, which is believed to have the effect of homogenizing the flow and is also believed to limit liquid transfer through the filter by allowing more drainage. This is supported by the higher drainage rates shown in Figure 6a in comparison to Figure 6b and that in Figure 6c compared to Figure 6d.

The pressure drop profile in Figure 6a shows two distinct steps corresponding to the saturation of the oleophobic media and then the oleophilic media, this step is less apparent in Figure 6b, likely due to the absence of the mesh layer between the two media types.

In Figures 6c,d, the increase in pressure drop is less immediate as the oleophilic media allow a depth filtration regime to exist until the media has become sufficiently saturated for the large coalesced droplets to form and impede the flow through the filter. By depth filtration, we are referring to the initial phase in classical dust filer, where the ΔP profile remains relatively unchanged during loading, as opposed to a surface filter where ΔP increases much more rapidly. This effect is not present in Figures 6a,b, where the media at the filter face is oleophobic, and therefore, does not allow aerosols to spread along the fibers during the early stages of filtration, as occurs in philic systems.[26] The depth filtration regime was also found in the Configuration 3 filter.

The evolution of the pressure drop in Figures 6c, d, where the oleophilic media is at the upstream filter face, can be seen to correspond to the stages of filtration described by Refs. [5] and [6].

As can be seen in Figure 7, the saturation in the last layer of the filter is higher for filters where the last layer is composed of philic media, likely due to the effect of hydrostatic forces, which act to push the oil to the rear of the filter.[4,27] The saturation in the final layer of Configurations 1A and 1B are higher than the other layers, with 1A slightly lower than 1B, likely due to the presence of the mesh reducing the hydrostatic pressure and/or increasing drainage. Lower saturation levels occurred in the rear filters in Configurations 2A and 2B, as these have the oleophobic filters at the rear. The lowest saturation levels occurred in Configuration 2B, and this is possibly due to the re-entrainment of droplets from the back of the filter into the gas stream.

Entrainment

During the Configuration B (no central mesh) experiments, droplet re-entrainment was observed. This is partly due to

Table 3. Gravimetric Efficiencies for Each Configuration

1A	2A	1B	2B	3
0.99990	0.99988	0.99974	0.96399	0.99999

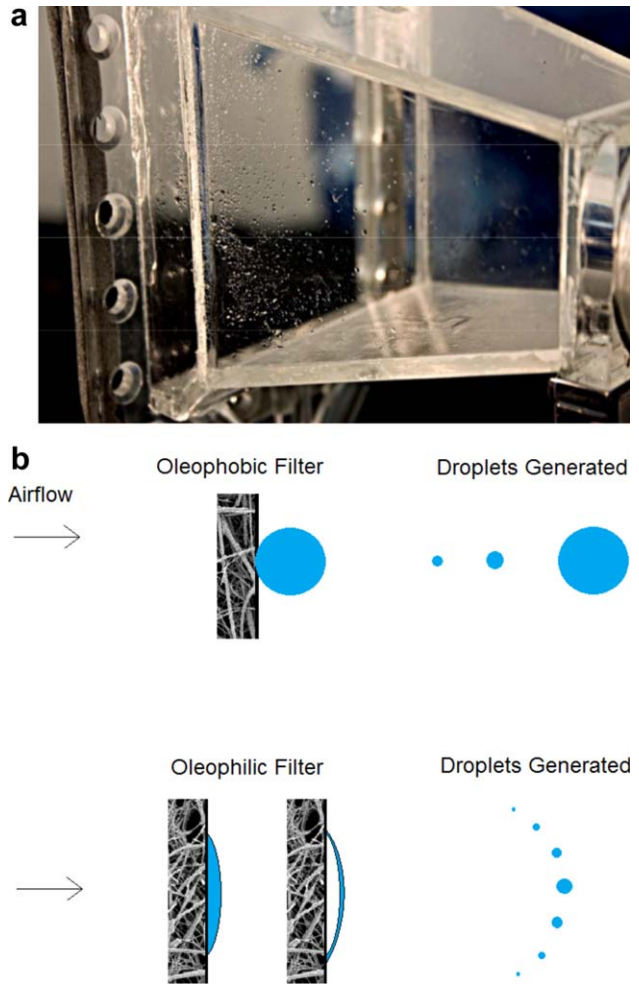

Figure 8. Droplet re-entrainment from the rear of the filter, (a) shows large droplets collected on the walls of the chamber downstream of the filter, (b) illustrates the proposed mechanism of satellite droplet formation.

[Color figure can be viewed in the online issue, which is available at wileyonlinelibrary.com.]

the significantly higher pressure drops attained in these experiments. This re-entrainment (or "blow off") was significantly more pronounced in case 2B, where the rear filter layers were oleophobic. This is due to the weaker droplet fiber adhesion forces associated with the "clamshell" droplets that form on "nonwettable" materials.[10]

Figure 8a shows part of the filter chamber downstream from the filter, after the 2B experiments. Large oil droplets may be seen on the walls of the chamber, where large droplets that were re-entrained have been deposited. The OPC detected some aerosols after the filter, which were larger than the largest droplet size before the filter, which supports the presence of re-entrainment. It is, however, suspected that the aerosol detected by the OPC were only satellite droplets for the large (undetectable) droplets, which deposited on the chamber after the filter, visible in Figure 8. The largest size measurable by OPC is ~10 μm. Based on our observation, a conceptual mechanism for entrainment (or re-entrainment) from phobic and philic media is shown in Figure 8b. However, it should be noted that these mechanisms represent a hypothesis based on qualitative observation, and the relative contribution (or indeed merit) of each mechanism remains to be tested. Indeed, to our knowledge, no previous literature has examined such entrainment, apart from Ref. [1], who developed a novel measurement approach, however, did not detect entrainment in their filters.

Due to the broad particle size and comparatively low concentration of re-entrained aerosol, it is difficult to measure. To attempt a first measurement, a CPC (TSI 3010) was used separate from the SMPS system, and with the nebulizer disconnected, so no influent aerosol was present. Figure 9 shows entrained particles produced by filters 1B and 2B. These particles must be in the range of 10 nm to ~2.5 μm,[28] which represent the detection limits of the device. SMPS measurements of the re-entrained aerosol spectra proved unreliable, suggesting that most particles were $\leq$ 50 nm and were subject to evaporation in the SMPS sheath air (as found in previous work[24]). Note that this effect is likely insignificant for the high concentration aerosols during standard filter testing experiments. The difference between the data for 1B and 2B, in Figure 9, was shown to be significantly different using a *t*-test ($P < 0.0001$).

Given the pressure drop and efficiency results, it appears that the use of a supporting mesh within the filter is beneficial in terms of both structural integrity and in minimizing the pressure drop. The use of oleophobic filter layers at the front of the media seems to offer improved filter efficiency while the use of such media at the rear of the filter may lead to re-entrainment, though this effect has been proven to exist for both the philic and phobic media.

Comparison with Saturation Models and Quality Factor Determination

Filter quality factor (Q_f) can be defined as[29]

$$Q_f = \frac{\ln\left(\frac{1}{P}\right)}{\Delta P} \tag{2}$$

where P is filter penetration (in this case overall mass-based fractional penetration, which may be determined from the

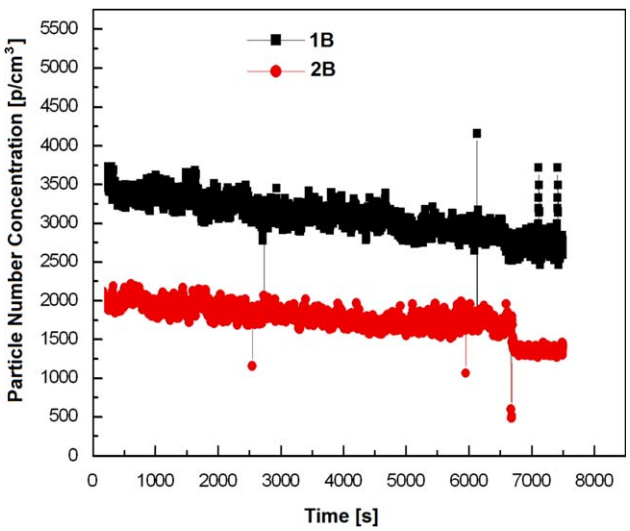

Figure 9. Measured small droplet re-entrainment for the case B configurations.

[Color figure can be viewed in the online issue, which is available at wileyonlinelibrary.com.]

Table 4. Q_f Values and Experimental and Calculated Saturation Values for the Filter Configurations

Configuration	Q_f (1/mBar)	S_F (−)	$S_{mod\,1}$ (26[a])	$S_{mod\,2}$ (28[a])	$S_{mod\,3}$ (9[ab])
1A	0.151	0.629	0.183	0.553	0.72
1B	0.087	0.698	0.183	0.107	0.56
2A	0.099	0.591	0.183	0.322	0.64
2B	0.030	0.526	0.183	0.018	0.53
3	0.096	0.723	0.043	∼0	0.24

[a]Equation numbers from Ref. [2]
[b]Eq. 9 from Ref. [2] determines a capillary rise height, which can then be converted to a saturation value.

values given in Table 3). Although Q_f has limited applicability as it is only useful in comparing filters of the same surface area (and for mist filters the same aspect ratio also), it is nevertheless useful in this case to assist in choosing the best filter combination. Table 4 below shows the Q_f values for each filter in the study, with Configuration 1A clearly the best choice if Q_f is the most important criterion.

Although no empirical models exist to-date for phobic media (or philic–phobic combination media), it was considered a useful exercise to apply the models was recently developed for philic media.[2] Table 4 shows the overall experimental saturation values S_F, two empirical fits (Eqs. 26 and 28 in Ref. [2]), developed for 1–3 layer philic media, as well as the full capillary model (Eq. 9, as presented in Ref. [2]). It can be seen that the empirical fits do not agree well at all—apart from a reasonable agreement with 1A saturation for Eq. 28. The complete capillary model produces better agreement, though there is a significant deviation for Configuration 3, perhaps due to the thicker filter (five layers, two more than used to develop the model), and the fact that the capillary model does not consider changes in saturation profile through the media.

Conclusions

This work has examined the use of layers of oleophilic and oleophobic filter media with mesh supports. It was found that the use of the central mesh acted to minimize the pressure drop across the filter, promoting higher drainage rates, and reduced the re-entrainment of droplets from the filter. The presence of oleophobic media in combination with oleophilic media was found to change the effectiveness of the various mechanisms of particle capture, and therefore, the values of particle collection efficiency. The optimal configuration examined consisted of oleophobic media in the front, oleophilic media in the rear and a central mesh. In this configuration, any droplets that ordinarily may have been re-entrained from the rear of the oleophobic media were able to be drained from the mesh or were collected by the rear oleophilic layers. This configuration possessed a clearly superior Q_f value.

The re-entrainment of large droplets from the rear of filter configurations with oleophobic media as the final layer and high pressure drops was observed. It is clear that the phenomena of re-entrainment from mist filters require significant further study. Models to predict saturation in phobic (or combined philic–phobic) media need to be developed.

Finally, it is clear that gravimetric efficiency measurements and optical particle counting produce different results, especially when re-entrainment occurs.

Acknowledgment

This work was funded by the Australian Research Council and the DAAD-ATN Travel Grant Scheme.

Literature Cited

1. Raynor PC, Leith D. The influence of accumulated liquid on fibrous filter performance. *J Aerosol Sci*. 2000;31:19–34.
2. Mead-Hunter R, Braddock RD, Kampa D, Merkel N, Kasper G, Mullins BJ. The relationship between pressure drop and liquid saturation in oil-mist filters—predicting filter saturation using a capillary based model. *Sep Purif Technol*. 2013;104:121–129.
3. Frising T, Thomas D, Bémer D, Contal P. Clogging of fibrous filters by liquid aerosol particles: experimental and phenomenological modelling study. *Chem Eng Sci*. 2005;60:2751–2762.
4. Kampa D, Meyer J,Mullins BJ, Kasper G. A model for steady-state oil transport and saturation in a mist filter. In: *Proceedings of the 18th World IMACS and MODSIM09 International Congress on Modelling and Simulation: Interfacing Modelling and Simulation with Mathematical and Computational Sciences*, Cairns, Queensland, Australia 2009.
5. Charvet A, Gonthier Y, Gonze E, Bernis A. Experimental and modelled efficiencies during the filtration of a liquid aerosol with a fibrous media. *Chem Eng Sci*. 2010;65:1875–1886.
6. Contal P, Simao J, Thomas D, Frising T, Callé S, Appert-Collin JC, Bémer D. Clogging of fibre filters by submicron droplets. Phenomena and influence of operating conditions. *J Aerosol Sci*. 2004;35:263–278.
7. Liew TP, Conder JR. Fine mist filtration by wet filters–i. liquid saturation and flow resistance of fibrous filters. *J Aerosol Sci*. 1985;16:497–509.
8. Bredin A, Mullins BJ. Influence of flow-interruption on filter performance during the filtration of liquid aerosols by fibrous filters. *Sep Purif Technol*. 2012;90:53–63.
9. Bredin A, O'Leary RA, Mullins BJ. Filtration of soot-in-oil aerosols: why do field and laboratory experiments differ. *Sep Purif Technol*. 2012;96:107–116.
10. Mead-Hunter R, Bergen T, Becker T, O'Leary RA, Kasper G, Mullins BJ. Sliding/rolling phobic droplets along a fiber: measurement of interfacial forces. *Langmuir*. 2012;28:3483–3488.
11. Mullins BJ, Braddock RD. Capillary rise in porous, fibrous media during liquid immersion. *Int J Heat Mass Transfer*. 2012;55:6222–6230.
12. Park BH, Lee MH, Kim SB, Jo YM. Evaluation of the surface properties of PTFE foam coating filter media using xps and contact angle measurements. *Surf Sci*. 2011;257:3709–3716.
13. Mullins BJ, Braddock RD, Agranovski IE, Cropp RA, O'Leary RA. Observation and modelling of clamshell droplets on vertical fibres subjected to gravitational and drag forces. *J Colloid Interface Sci*. 2005;284:245–254.
14. Mullins BJ, Braddock RD, Agranovski IE. Particle capture processes and evaporation on microscopic scale in wet filters. *J Colloid Interface Sci*. 2004;279:213–227.
15. Kulkarni PS, Patel SU, Chase GG. Layered hydrophilic/hydrophobic fiber media for water-in-oil coalescence. *Sep Purif Technol*. 2012;85:157–164.
16. Agranovski IE, Myojo T, Braddock RD, Jarvis D. Combined wettable/non-wettable filter for mist purification. *Chem Eng Technol*. 2001;24:287–292.
17. Agranovski IE, Shapiro M. Clogging of wet filters as a result of drying. *Chem Eng Technol*. 2001;24:387–391.
18. Agranovski IE, Braddock RD. Filtration of liquid aerosols on non-wettable fibrous filters. *AIChE J*. 1998;44:2784–2790.
19. Agranovski IE, Shapiro M. Clogging of wet filters by dust particles. *J Aerosol Sci*. 2001;32:1009–1020.
20. Mullins BJ, Braddock RD, Agranovski IE, Cropp RA. Observation and modelling of barrel droplets on vertical fibres subjected to gravitational and drag forces. *J Colloid Interface Sci*. 2006;300:704–712.
21. Quere D, Di Meglio JM, Brochard-Wyart F. Wetting of fibers: theory and experiments. *Rev Phys Appl*. 1988;23:1023–1030.
22. Mead-Hunter R, Bredin A, King AJC, Larcher A, Becker T, Mullins BJ. The influence of soot nanoparticles on the micro/macro-scale behaviour of coalescing filters. *Chem Eng Sci*. 2012;84:113–119.
23. Sachweh B, Umhauer H, Ebert F, Büttner H, Friehmelt R. In situ optical particle counter with improved coincidence error correction for number concentrations up to 10^7 particles cm^{-3}. *J Aerosol Sci*. 1998;29:1075–1086.

24. Heim M, Mullins BJ, Umhauer H, Kasper G. Performance evaluation of three optical particle counters with an efficient "multimodal" calibration method. *J Aerosol Sci*. 2008;39:1019–1031.
25. Mullins BJ, Kampa D, Kasper, G. Comment on "performance evaluation of 3 optical particle counters with an efficient multimodal calibration method" (Heim et al., 2008)—performance of improved counter. *J Aerosol Sci*. 2012;49:48–50.
26. Mullins BJ, Agranovski IE, Braddock RD, Ho CM. Effect of fiber orientation on fiber wetting processes. *J Colloid Interface Sci*. 2004; 269:449–458.
27. Andan S, Harihanan SI, Chase GG. Continuum model evaluation of the effect of saturation on coalescence filtration. *Sep Sci Technol*. 2008;43:1955–1973.
28. Heim M, Kasper G, Reischi GP, Gerhart C. Performance of a new commercial electrical mobility spectrometer. *Aerosol Sci Technol*. 2004;38:3–14.
29. Chen CC, Willeke K. Aerosol penetration through surgical masks. *Am J Infect Control*. 1992;20:177–184.

Manuscript received Nov. 17, 2013, and revision received Mar. 13, 2014.